Journal of
Applied Crystallography
ISSN 0021-8898

Received 18 August 2000
Accepted 16 February 2001

Time-of-flight neutron transmission diffraction

J. R. Santisteban,[a]* L. Edwards,[a] A. Steuwer[b,c] and P. J. Withers[c]

[a]Department of Materials Engineering, The Open University, Milton Keynes MK7 6AA, England, [b]Department of Materials Science, University of Cambridge, Pembroke Street, Cambridge CB2 3QZ, England, and [c]Manchester Materials Science Centre, UMIST/University of Manchester, Grosvenor Street, Manchester M1 7HS, England. Correspondence e-mail: j.r.santisteban@open.ac.uk

The positions of Bragg edges in neutron transmission experiments can be defined with high accuracy using the time-of-flight (TOF) technique on pulsed neutron sources. A new dedicated transmission instrument has been developed at ISIS, the UK spallation source, which provides a precision of $\Delta d/d \simeq 10^{-5}$ in the determination of interplanar distances. This is achieved by fitting a theoretical three-parameter expression to the normalized Bragg edges appearing in the TOF transmission spectra. The technique is demonstrated by experiments performed on iron, niobium and nickel powders. The applicability of using the instrument for the determination of lattice strains in materials has been investigated using a simple *in situ* loading experiment. Details of the calibration process are presented and the dependence of the resolution and the experimental times required by the transmission geometry on the instrumental variables are studied. Finally, the requirements for a Rietveld-type refinement of transmission data and the advantages and limitations over traditional neutron diffraction peak analysis are discussed.

1. Introduction

The high counting rate and statistical quality of neutron transmission experiments at intense pulsed neutron sources such as ISIS and LANSCE have opened the possibility for new studies in materials science, including measurements of residual stresses (Wang, 1996), kinetics of phase transformations (Meggers *et al.*, 1994), fast measurements of temperature (Mayers *et al.*, 1989) or hydrogen-content determination (Granada *et al.*, 1995).

In this paper, we focus on the sharp discontinuities that appear in the total neutron cross section of polycrystalline materials as a result of coherent elastic scattering on the lattice planes, which are clearly seen in the cross section of iron displayed in Fig. 1. These 'Bragg edges' occur because, for a given *hkl* reflection, the Bragg angle increases as the wavelength increases until 2θ is equal to 180°. At wavelengths greater than this critical value, no scattering by this particular $\{hkl\}$ family can occur and there is thus an increase in transmitted intensity. From Bragg's law, the wavelength at which this occurs is $\lambda = 2d_{hkl}$, giving a measure of the $\{hkl\}$ d spacing in the direction of the incoming beam.

Mathematically, the coherent elastic cross section may be expressed as an infinite sum of heaviside step functions $\theta(\lambda)$, one associated with each reflection

$$\sigma_{\rm coh}(\lambda) = \sum_{hkl} \sigma_{hkl}(\lambda)[1 - \theta(\lambda - 2d_{hkl})], \qquad (1)$$

with $\sigma_{hkl}(\lambda)$ being the partial contribution of the $\{hkl\}$ family of planes.

In order to define the position of the Bragg edges to a high precision, it is necessary to provide a model describing the broadening of the edges introduced by the finite resolution of the instrument. This has been already described for the cases of a steady-state reactor coupled with a position sensitive detector (Strunz *et al.*, 1997) and for a pulsed reactor using a Fourier chopper (Hiismäki, 1988). In this paper we consider the case of TOF transmission experiments on spallation sources.

We propose here a three-parameter profile to describe the Bragg edge, which is used to calibrate a new dedicated instrument based at ISIS, UK. The capability of this new instrument for neutron strain scanning has been investigated by *in situ* measurements during tensile and compressive tests on a steel specimen. In addition, the precision of the instrument has been evaluated using niobium and copper powders. Finally, the systematic and statistical errors of the technique are discussed, and the optimal thickness of a given material for lattice-parameter determination is derived.

2. Basic concepts

In an idealized case, a TOF transmission instrument comprises a pulsed point neutron source and a point detector, placed at a distance l, which counts the number of neutrons $N(t) = I(t)\Delta t$ arriving between times t and $t + \Delta t$ after the pulse. The number of neutrons transmitted by the sample, $N_{\rm in}$, is compared with the corresponding number of neutrons counted with the sample removed, $N_{\rm out}$, as a function of the neutron wave-

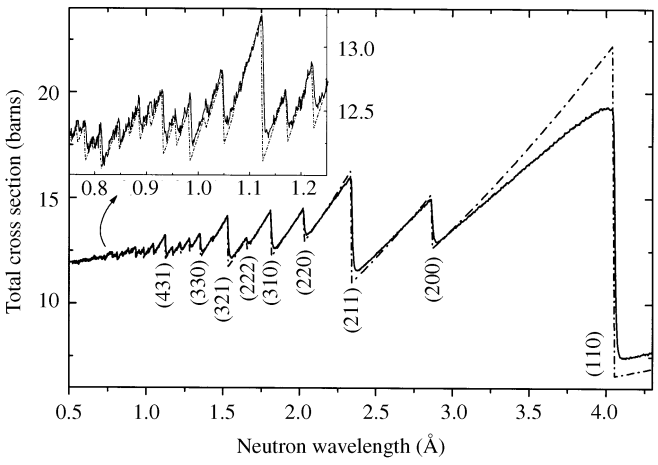

Figure 1
Total cross section of iron powder, displaying characteristic Bragg edges: experimental values measured at ENGIN, ISIS (solid line); values for an ideal powder calculated using the code *CRIPO* (Kropff & Granada, 1975) (dash-dot line). The difference in intensity in the first Bragg edge is caused by extinction effects.

length. Because of the different velocities, neutrons with wavelength λ arrive at the detector with a TOF t given by

$$t = (ml/h)\lambda, \tag{2}$$

allowing a direct transformation between TOF and wavelength.

In reality, at a pulsed spallation source, the high-energy neutrons created by spallation are moderated by collisions with the light atoms within the moderator. The resulting uncertainty in the time and position at which the neutron leaves the moderator prevents precise determination of the TOF and flight path of the detected neutron. As a result, for a fixed neutron wavelength there is a resolution function $R(\lambda, t)$ describing the number of neutrons arriving at the detector.

A pulsed source produces neutrons with a very broad wavelength distribution $S(\lambda)$, so to calculate the number of neutrons detected between t and $t + \Delta t$ we have to consider the neutrons of all wavelengths arriving during that interval,

$$N_{\rm in}(t) = I_{\rm in}(t)\Delta t = \Big[\int_0^\infty S(\lambda')\,{\rm Tr}(\lambda')\,\varepsilon(\lambda')\,R(\lambda', t)\,{\rm d}\lambda'\Big]\Delta t, \tag{3}$$

where $\varepsilon(\lambda')$ is the detector efficiency for neutrons of wavelength λ' and ${\rm Tr}(\lambda')$ is the transmission of the sample, given by

$${\rm Tr}(\lambda') = \exp[-nw\sigma_{\rm tot}(\lambda')], \tag{4}$$

where w is the sample thickness, n is the number of atoms per unit volume and $\sigma_{\rm tot}(\lambda')$ is the total cross section of the sample. To obtain the analytical expression for the broadening of the Bragg edge, we isolate in the total cross section the contribution σ_{hkl} for the family of planes we are interested in:

$$\sigma_{\rm tot}(\lambda') = \sigma_0(\lambda') + \sigma_{hkl}(\lambda')[1 - \theta(\lambda' - 2d_{hkl})], \tag{5}$$

with $\sigma_0(\lambda')$ accounting for contributions other than the elastic coherent scattering of the current *hkl*. Provided that $S(\lambda')$, $\varepsilon(\lambda')$ and the cross section $\sigma_0(\lambda')$ are flat functions within the very narrow integration interval defined by the sharply peaked function $R(\lambda', t)$, we can approximate the result by taking them outside the integral:

$$I_{\rm in}(t) \simeq S(\lambda_t)\,\varepsilon(\lambda_t)\,\exp[-nw\sigma_0(\lambda_t)] \times \int_0^\infty \exp\{-nw\sigma_{hkl}(\lambda')[1 - \theta(\lambda' - 2d_{hkl})]\}\,R(\lambda', t)\,{\rm d}\lambda', \tag{6}$$

with λ_t given by equation (2). Introducing explicitly the step function in the integral limits and using the fact that $\sigma_{hkl}(\lambda')$ is also a slowly varying function, we obtain, after a little algebra, the final form for the normalized transmitted intensity:

$$I_{\rm in}(t)/I_{\rm out}(t) = \exp[-nw\sigma_0(\lambda_t)]\Big(\exp[-nw\sigma_{hkl}(\lambda_t)] + \{1 - \exp[-nw\sigma_{hkl}(\lambda_t)]\}\int_{2d_{hkl}}^\infty R(\lambda', t)\,{\rm d}\lambda'\Big). \tag{7}$$

Thus, the exact shape of the Bragg edge will depend on the resolution function of the instrument. In this work we adopt one of the simplest models for $R(\lambda, t)$, namely that proposed by Kropff *et al.* (1982), consisting of a Gaussian of deviation $\sigma(\lambda)$ convoluted with a decaying exponential starting at a time $t_0(\lambda)$ and decaying with a time constant $\tau(\lambda)$:

$$R(\lambda, t) = \theta(t - t_0)\frac{1}{\tau}\exp\Big(-\frac{t - t_0}{\tau}\Big) \otimes \frac{1}{(2\pi)^{1/2}\sigma}\exp\Big[-\frac{(t - t_0)^2}{2\sigma^2}\Big] = \frac{1}{2\tau}\exp\Big(-\frac{t - t_0}{\tau} + \frac{\sigma^2}{2\tau^2}\Big){\rm erfc}\Big(-\frac{t - t_0}{2^{1/2}\sigma} + \frac{\sigma}{\tau}\Big). \tag{8}$$

The advantage of this peak shape is that it can be integrated analytically, providing an easy-to-fit three-parameter expression (t_0, σ, τ) of the normalized Bragg edge. The capability of the Kropff model to describe the diffraction peaks obtained at ISIS is illustrated in Fig. 2(*a*), which shows a fit to the (110) peak from an iron powder. After solving the integral, the resulting line shape is

$$B(d_{hkl}, t) = \int_{2d_{hkl}}^\infty R(\lambda', t)\,{\rm d}\lambda' = \frac{1}{2}\Big[{\rm erfc}\Big(-\frac{t - t_{hkl}}{2^{1/2}\sigma}\Big) - \exp\Big(-\frac{t - t_{hkl}}{\tau} + \frac{\sigma^2}{2\tau^2}\Big){\rm erfc}\Big(-\frac{t - t_{hkl}}{2^{1/2}\sigma} + \frac{\sigma}{\tau}\Big)\Big], \tag{9}$$

where t_{hkl} is the TOF when neutrons of wavelength $2d_{hkl}$ arrive at the detector. This function, $B(d_{hkl}, t)$, describes the broadening of Bragg edges in TOF transmission very well, as can be seen in Fig. 2(*b*) which shows the excellent fit achieved to the 110 Bragg edge from the iron powder. More complex analytical expressions for the Bragg edge may also be derived from the resolution function proposed by Carpenter *et al.* (1975), consisting of the convolution of a Gaussian with two back-to-back exponentials. Vogel (2000) has implemented such a model in a Rietveld code and used it to study time-resolved phase transformations. No improvements in the fits of the experimental data collected in this work were found by adopting such a model.

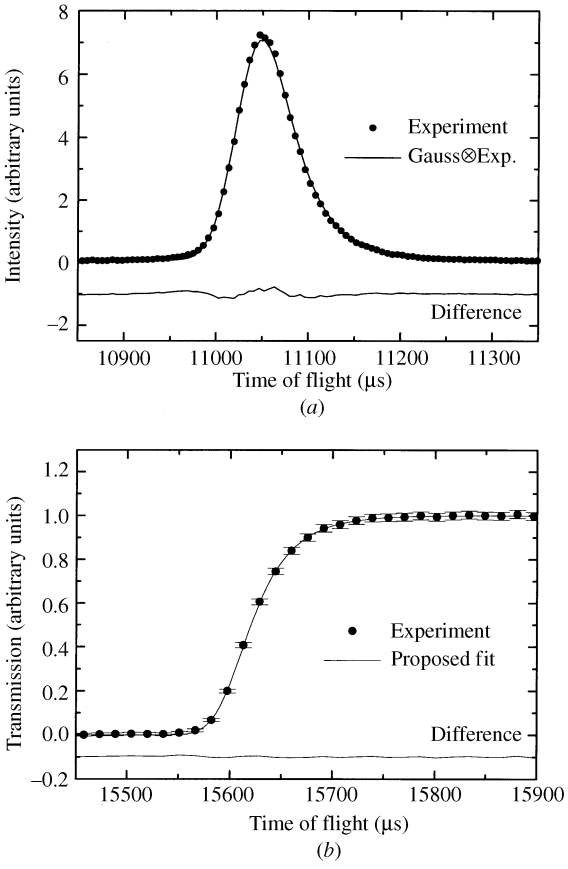

Figure 2
(*a*) Experimental 110 Bragg diffraction peak in iron powder and least-squares fit using the convolution of an exponential with a Gaussian function (solid line). (*b*) Experimental 110 edge in iron powder and least-squares fit using the line shape proposed in this work. Both spectra were acquired at ISIS on the ENGIN instrument at the same time, but the peaks have different times of flight because of the scattering angles (2θ = 90 and 180° for diffraction and transmission, respectively).

3. Calibration

In order to calibrate the diffractometer in terms of *d*-spacing scale, we have used a standard polycrystalline sample to evaluate the dependence of the instrumental parameters t_{hkl}, σ and τ on neutron wavelength. Iron powder was selected as a calibration standard because of its high coherent cross section and because its body-centred cubic (b.c.c.) structure produces several well separated Bragg edges. These instrumental parameters have been compared with their Bragg diffraction equivalent, derived from simultaneous conventional diffraction experiments. Experiments on a 99%-pure powder contained within a 25 × 25 × 25 mm thin-walled vanadium box were performed on the ENGIN instrument position of the PEARL beamline at ISIS, UK. This beamline 'sees' the central part of a 45 mm thick 115 × 115 mm liquid-methane moderator at an angle of 12°. The transmitted spectrum was recorded using a 50 mm^2 scintillating glass detector, with 10% efficiency ε at λ = 1 Å over a counting time of 4 h. A variable time channel Δt was used to keep the resolution at a constant value of $\Delta t/t$ = 0.001. The conventional diffraction Bragg spectra were measured using the ENGIN 90° detectors, which were specially designed to measure strains and hence stresses in engineering materials (Johnson *et al.*, 1997).

After indexing the edges observed in transmission and the peaks in diffraction, the corresponding neutron wavelength scales were defined using Bragg's law and the cell parameter of the iron standard, 2.8665 Å (*CRC Handbook of Chemistry and Physics*, 1997), to calculate the wavelength associated with each individual reflection. The eight most intense Bragg edges (110, 200, 211, 220, 310, 321, 330 and 431 in Fig. 1) were fitted individually using the expression given by equation (7) in a least-squares refinement procedure. For the purposes of the fitting, the cross sections $\sigma_0(\lambda)$ and $\sigma_{hkl}(\lambda)$ were approximated by linear functions within a narrow time interval including the edge. Thus, the actual expression describing the transmission near a Bragg edge is given by

$$N_{\rm in}(t)/N_{\rm out}(t) = \exp[-(a_0 + b_0 t)]\big(\exp[-(a_{hkl} + b_{hkl} t)] + \{1 - \exp[-(a_{hkl} + b_{hkl} t)]\} B(t_{hkl}, \sigma, \tau, t)\big), \quad (10)$$

with $B(t_{hkl}, \sigma, \tau, t)$ given by equation (9). In order to avoid local minima, the fitting was carried out in three stages. Firstly, the parameters a_0 and b_0 were defined from the values of the transmission on the far-right side of the edge [where $B(t_{hkl}, \sigma, \tau, t) = 1$]; equation (10) becomes

$$N_{\rm in}(t)/N_{\rm out}(t) = \exp[-(a_0 + b_0 t)]. \quad (11)$$

Secondly, the parameters a_{hkl} and b_{hkl} describing the jump in the cross section were defined by keeping a_0 and b_0 fixed and fitting the data on the far-left side of the edge [where $B(t_{hkl}, \sigma, \tau, t) = 0$]; the transmission is given by

$$N_{\rm in}(t)/N_{\rm out}(t) = \exp[-(a_0 + b_0 t)] \exp[-(a_{hkl} + b_{hkl} t)]. \quad (12)$$

Finally, the values of t_{hkl}, σ and τ were defined from least-squares fitting where the values of a_0, b_0, a_{hkl} and b_{hkl} were fixed. The normalized transmission displayed in Fig. 2(*b*) was obtained by extracting the experimental $B(t_{hkl}, \sigma, \tau, t)$ after completing the second stage.

While t_{hkl} follows an almost perfect linear law with neutron wavelength, the results of Figs. 3(*a*) and 3(*b*) show that the parameters τ and σ display a slightly more complex dependence. A linear regression of the values of t_{hkl} against neutron wavelength allowed the definition of the neutron flight path l appearing in equation (2) [1522.66 (27) cm], providing the calibration of the TOF wavelength scale.

The decay constant τ is a characteristic property of the moderator, depending on its geometry and the temperature; it is expected to be the same in both transmission and diffraction. Very good agreement between the results from both diffraction geometries can be seen in Fig. 3(*a*), with the exponential constant displaying the step-like behaviour observed by Kropff *et al.* (1982). As a result of this calibration process, we can establish an analytical expression for the decay constant of the moderator as a function of λ; thus, the values of τ (μs) between 1 and 4.1 Å have been empirically fitted by

$$\tau(\lambda) = \mathrm{erfc}[(\lambda - \lambda_0)/\Delta](A + B\lambda), \quad (13)$$

with λ_0 = 1.02 Å, Δ = 0.55 Å, A = 27.8 μs and B = 1.75 μs $Å^{-1}$.

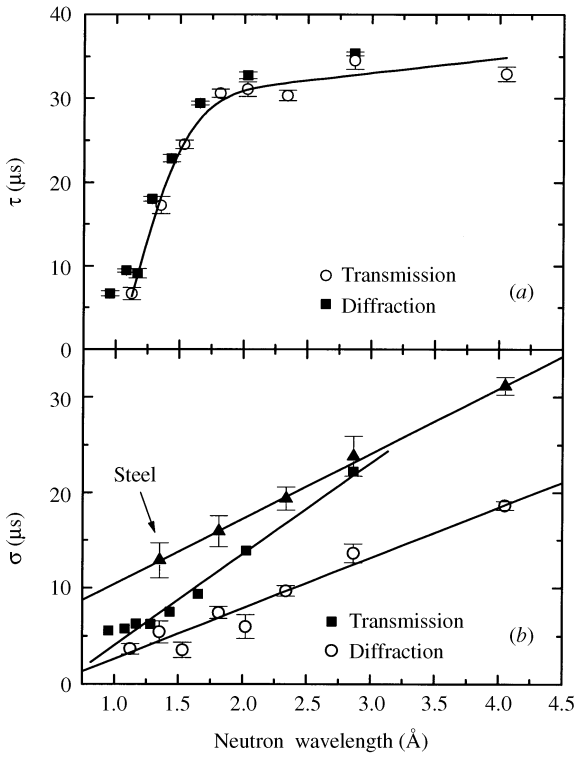

Figure 3
(*a*) Moderator decay constant τ as a function of neutron wavelength defined with respect to diffraction and transmission geometries. The solid line is an empirical fit to the transmission data. (*b*) Gaussian broadening σ for iron powder and ferritic steel in transmission and diffraction geometries. The error bars for the diffraction data are smaller than the symbols. The lines are linear fits to the data.

In contrast, the Gaussian broadening σ depends on the sample as well as on the instrumental setup and is smaller in transmission than in diffraction as a result of the angular uncertainty present in the latter case. This is because the sample thickness, which is important in diffraction, does not contributes to the broadening in transmission, as the transmitted neutrons all have the same flight path. The smaller broadening in transmission is clear in Fig. 3(*b*), which plots values of σ emerging from both geometries. In a pure powder, the main contribution to σ comes from instrumental contributions, which in a first approximation present a linear dependence with respect to neutron wavelength. From linear fits, the average values of (σ/t_{hkl}) obtained were 0.0014 in transmission and 0.0024 in diffraction. In addition to the referred geometrical broadening, there is also a microscopic broadening of the total cross section caused by the distribution of d spacings within the sample as well as crystal size effects, which is exemplified in Fig. 3 by the higher values obtained in transmission for a 6 mm thick low-carbon steel sample.

4. Trial experiments

Two experiments were performed in order to test the sensitivity and precision of the instrument. In the first experiment, the sensitivity was explored by measuring the Poisson ratio of a low-carbon steel, whereas in the second the precision was investigated through the determination of the lattice parameters of niobium and nickel powders.

For the definition of the Poisson ratio (ν), a 6 mm thick, 6 mm wide and 80 mm long EN8 (0.42 wt% C, 0.64 wt% Mn) steel sample was mounted in a tensile stress rig and subjected to different loads applied perpendicular to the beam direction. The strain parallel to the applied load $\varepsilon_{\|}$ was measured by a strain gauge attached to the sample, while the strain perpendicular to the load, $\varepsilon_{\perp} = -\nu\varepsilon_{\|}$, was defined by Bragg-edge analysis from the change in the interplanar distance d relative to the unstressed value d_0:

$$\varepsilon_{\perp} = (d - d_0)/d_0 = \Delta d/d_0. \qquad (14)$$

A similar experiment was performed for compression using a 10 × 10 × 25 mm sample from the same parent material inserted into a special compression rig (Wang, 1996). All the applied strains, $\varepsilon_{\|} = \pm 1000\ \mu\varepsilon$, $\pm 1850\ \mu\varepsilon$ ($1\ \mu\varepsilon = 10^{-6}$) were within the elastic regime of the material. Taking $\nu \simeq 0.3$ for steel, the strains perpendicular to the load were expected to be of the order of 10^{-4}, representing a severe test for the sensitivity of the technique. The experiments were performed under the same experimental conditions used in the calibration. The counting times were 2.8 h and 1.1 h per spectrum for the compressive and tensile tests, respectively. The edges were fitted using the procedure described in the previous section, varying the Bragg edge position t_{hkl} and the Gaussian broadening σ, while the exponential decay time τ was fixed at its calibration value. The capability of the TOF technique to simultaneously record many reflections allowed the study of the dependence of the Poisson ratio on the particular (*hkl*) reflection resulting from the anisotropy of the sample. Fig. 4 shows this dependence through plots of individual strains measured for the 110, 200 and 211 reflections. Data from the 310 and 321 reflections are omitted from this graph to aid visualization. The values of the Poisson ratio resulting from least-squares linear fittings were $\nu_{110} = 0.233\,(7)$, $\nu_{200} = 0.41\,(1)$, $\nu_{211} = 0.280\,(8)$, $\nu_{310} = 0.31\,(5)$ and $\nu_{321} = 0.22\,(3)$, decreasing monotonically with the anisotropy parameter Γ, as expected from theoretical considerations (Windsor & Izuyama, 1992). In order to compare these results with available information on the Poisson ratio, the individual strains were weight-averaged to produce a unique strain that one would expect to be closer to the macroscopic properties of the material. This average strain is plotted in the inset of Fig. 4; the Poisson ratio resulting from the fitting was $\nu = 0.284\,(5)$, a reasonable value for this ferritic steel (*Smithells Metals Reference Book*, 1983).

In the previous example, only changes in elastic strain were expected as a result of the application of applied loads. Provided that the measured strains were proportional to the relative shift of the Bragg edges, the loading experiment was a good test of the sensitivity of the diffractometer, but not of the uncertainty of the technique for measuring interplanar distances in a more general situation. For instance, when the sample thickness or the material is changed, the transmitted spectra become notably different from each other. Thus, an

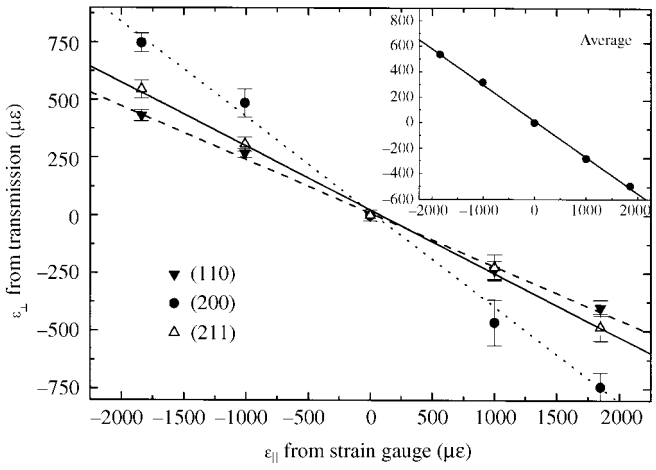

Figure 4
Relation between the strain $\varepsilon_{\|}$ in the direction of the applied load and the Poissson strain $\varepsilon_{\perp}$ in the normal direction for a low-carbon steel. The analysis of the individual edges shows the change in the Poisson ratio as a result of the anisotropy of the material. The average normal strain of the five largest edges is displayed in the inset.

estimation of the precision in d spacing achievable in transmission experiments can be obtained by measuring the lattice parameter of reference samples of different materials. This has been done for Ni and Nb powders using samples having effective thicknesses of 10.3 mm and 15.9 mm, respectively. The experiment was performed using a 9 mm^2 50%-efficiency (at 1 Å) scintillating detector; the counting times were 3 h for Ni and 4 h for Nb. The measured total cross sections are presented in Fig. 5; the lattice parameters resulting from the first Bragg edge, 111 in Ni and 110 in Nb, were $a_{\rm Ni}$ = 3.5239 (1) Å and $a_{\rm Nb}$ = 3.3002 (1) Å, in excellent agreement with the values $a_{\rm Ni}$ = 3.5240 Å and $a_{\rm Nb}$ = 3.3004 Å reported in the literature (*CRC Handbook of Chemistry and Physics*, 1997). Errors were estimated from the standard deviation of the parameter t_{hkl}, given by the square root of the diagonal elements of the variance–covariance matrix in the least-squares fitting routine. The error discussed here represents only the statistical uncertainty in the fitting process and does not account for any systematic errors in the experimental procedure, a fact that comes to light when the previous values are compared with the lattice parameter given by other reflections, *i.e.* $a_{\rm Ni}$ = 3.5245 (2) Å and $a_{\rm Nb}$ = 3.3007 (1) Å if the 220 and 211 reflections are used for Ni and Nb, respectively. The reason for the difference between the values (∼170 με) will be explained in next section; however, it is worth pointing out that the edges used in the first analysis were chosen to minimize possible systematic errors.

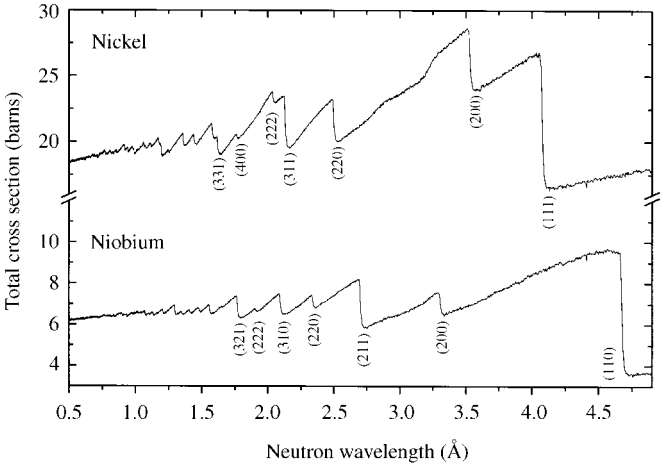

Figure 5
Experimental total cross sections of nickel and niobium. The lattice parameters obtained from the Bragg-edge analysis using only the first Bragg edge were 3.5239 (1) and 3.3002 (1) Å, respectively.

5. Systematic errors

In §3, we assumed that all neutrons leave the moderator at the same time and adopted the simple relationship given by equation (2) to describe the relation between the edge position t_{hkl} and its associated neutron wavelength. In fact, in TOF transmission experiments, neutrons of many wavelengths contribute to the same time channel so that inferring an associated wavelength is not straightforward. However, equation (2) can be seen as a good approximation to the relation linking the TOF channel $(t, t + \Delta t)$ to the mean wavelength of all the neutrons arriving within that interval. The effect of different emission times for neutrons detected at different time channels is detectable using the present instrument and can be seen in Fig. 6(*a*), where the lattice parameter resulting from the fit of different edges is plotted as a function of neutron wavelength. The values present a systematic V-shaped dependence on neutron wavelength, a behaviour also observed in the analysis of the Bragg diffraction data. The largest difference in a_0 found in transmission was equivalent to approximately 800 με between the 110 and 321 edges, which is an order of magnitude larger than the statistical error of the fits. To overcome this problem, the real TOF of the neutron t must be extracted from the time recorded in the experiment, $t_{\rm exp}$, by subtracting the wavelength-dependent emission time of the neutron $t_{\rm emi}(\lambda)$. By assuming a linear dependence of $t_{\rm emi}$ on λ, the only difference from the former calibration consists of the inclusion of a fixed term in the linear regression:

$$t = (ml'/h)\lambda + t_0, \qquad (15)$$

where the flight path l has changed to an effective flight path l' because it also includes the linear term for the correction. By including this correction, the scatter in lattice parameter between 1.3 and 4.1 Å is considerably reduced and the experimental points adopt a random distribution around the mean value. However, this model is too simple to account for the rise of the lattice parameter at wavelengths shorter than 1.3 Å, and a more elaborate description of $t_{\rm emi}(\lambda)$ should be adopted if a wider range is to be exploited. No significant improvement was found by using a quadratic relation between TOF and neutron wavelength.

The three-stage fitting procedure described in §3 is very important for avoiding systematic errors in the edge parameters introduced by the appearance of local minima in the

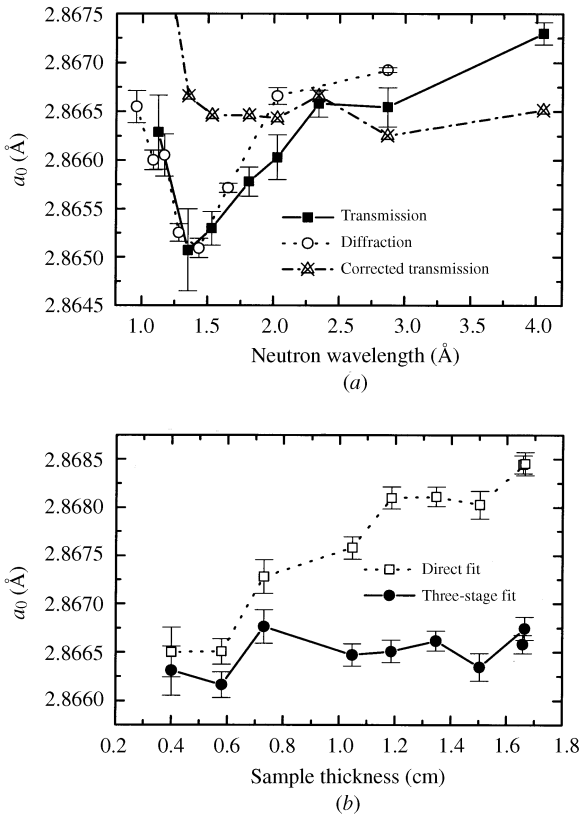

Figure 6
Systematic errors in the determination of the lattice parameter of iron powder. (*a*) Change with neutron wavelength caused by the effect of the varying emission time of the neutron seen in both transmission and diffraction geometries. (*b*) Change introduced by changing the sample thickness. The effect is corrected when the three-stage fitting procedure proposed in this work is adopted.

least-squares surface. As an example of such systematic errors, Fig. 6(*b*) shows the lattice parameter of iron powder resulting from the 211 edge in samples of different thickness. When the 'direct fitting' was performed, *i.e.* when the seven parameters describing the transmission near the edge were fitted within the same time interval, the increase in the attenuation of the beam introduced a pseudo-strain of 50 $\mu\varepsilon$ mm^{-1}. By contrast, no noticeable shift was observed when the fitting procedure proposed in this work was adopted. This result is important for the application of neutron transmission to problems involving changes in the effective thickness along the beam direction, as for example in the determination of the unstressed lattice parameter as proposed by Steuwer *et al.* (2000).

6. Optimal configuration

Optimization of the experimental arrangement requires the definition of a figure of merit, the study of its dependence on relevant experimental parameters, and its maximization for the parameters likely to be modified in the experimental setup. Because, in our case, some parameters affecting the instrumental resolution, such as the moderator-dependent decay constant τ, are already fixed, the problem is reduced to the following basic questions: (i) where should the detector be placed, (ii) how long should one count, and (iii) what is the best sample thickness? This section is aimed at answering these questions and at predicting the performance of the transmission technique for different materials. This enables future experiments to be planned. For example, we can optimize sample thickness to obtain the best achievable resolution in d spacing.

The uncertainty in the definition of the edge position Δd is inversely proportional to the edge height h and directly proportional to its uncertainty Δh. Using Poisson statistics to describe the mean-square statistical fluctuation in the number of neutrons detected within a time channel, the proportionality can be expressed in terms of the number of neutrons counted within the time channels on the left and right sides of the edge:

$$(\Delta d)^2 = K(\Delta h/h)^2 = K(N_{\rm right} + N_{\rm left})/(N_{\rm right} - N_{\rm left})^2. \quad (16)$$

The number of neutrons counted by the detector is

$$N_{\rm left,right} = {\rm Tr}_{\rm left,right}\,\Phi(\lambda)\,\varepsilon(\lambda)\,A\,T_c\,|\partial\lambda/\partial t|\,\Delta t, \quad (17)$$

where $\mathrm{Tr}_{\rm left,right}$ is the transmission of the sample at the left and right sides of the edge, respectively, $\Phi(\lambda)$ is the differential neutron flux at the sample position (neutrons Å^{-1} cm^{-2} s^{-1}), A and $\varepsilon(\lambda)$ are the detector area and efficiency, respectively, T_c is the elapsed counting time (s), Δt is the channel width and $|\partial\lambda/\partial t|$ is the Jacobian between λ and t. If we assume no collimation in the beam, the neutron flux can be expressed in terms of the flux $\Phi_0(\lambda)$ at a distance l_0 from the source, $\Phi(\lambda) = \Phi_0(\lambda)(l_0/l)^2$. For the ENGIN instrument, we estimate a value of 63 000 neutrons Å^{-1} cm^{-2} s^{-1} for wavelengths close to the first Bragg edge in iron (4 Å). Expressing the transmission of the sample at both sides of the edge in terms of the atomic density, the microscopic cross sections and the sample thickness, we obtain

$$\left(\frac{\Delta d}{d}\right)^2 = K\frac{l\exp(nw\sigma_0)}{\Phi_0(\lambda)\,l_0^2\,\varepsilon(\lambda)\,A\,T_c\Delta t}\frac{[1+\exp(-nw\sigma_{hkl})]}{[1-\exp(-nw\sigma_{hkl})]^2}, \quad (18)$$

where σ_{hkl} and the total cross section σ_0 can be calculated (Kropff & Granada, 1975) or obtained from nuclear databases. This equation suggests that as long as the edges of interest do not overlap and the dimensions of the detector are negligible compared with the flight path, the detector should be located as close as possible to the neutron source. The precise value of the proportionality constant K in equation (18) depends on the parameters τ and σ defining the broadening of the edge, but according to Figs. 3(*a*) and 3(*b*), K is not expected to change greatly for neutron wavelengths in the range 1.8–5.0 Å. The value of K was estimated from the experimental uncertainty observed in the calibration experiments, and it was used to predict the precision $\Delta d/d$ for different materials, shown in Fig. 7. These estimates correspond to the analysis of the first Bragg edge, recorded with a 4 mm^2 detector placed 15 m from the neutron source and counting for 1 h with a time channel of 16 µs width. As seen from the graph, the uncertainty in the edge determination ultimately depends on the specific mate-

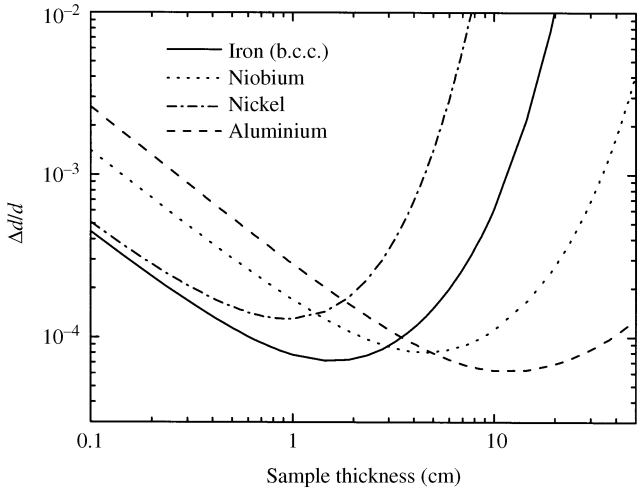

Figure 7
Dependence of the resolution of the transmission diffractometer on sample thickness for different materials. The calculation was made for a 4 mm^2 detector, placed at 15 m from the moderator, after 1 h of counting time and is based on analysing just the first Bragg edge. Better results would be achieved by refining the lattice parameter based on a multiple-edge refinement.

rial, but for thicknesses between 1 and 5 cm, all the resolutions are between 10^{-4} and 10^{-5}. The optimal sample thickness can be found by simple minimization of equation (18), obtaining

$$w_{\rm opt} = \frac{1}{n\sigma_{hkl}} \ln \left\{ \frac{3}{2}\frac{\sigma_{hkl}}{\sigma_0} + \left[\left(\frac{3}{2}\frac{\sigma_{hkl}}{\sigma_0} \right)^2 + \frac{\sigma_{hkl}}{\sigma_0} + 1 \right]^{1/2} \right\}. \quad (19)$$

The optimal sample thickness and the precision expected in this case for 1 h counting using a 4 mm^2 detector for some common materials are presented in Table 1. As an example of the use of expression (18) to estimate the counting time required for a given experiment, we have included in Table 1 the time necessary to produce a resolution of 10^{-4} using a 400 mm^2 detector when samples of optimal and 5 mm thickness are measured.

7. Discussion

In this work we have shown that by fitting an appropriate line shape to the Bragg edges, it is possible to define interplanar distances with a resolution of 30 $\mu\varepsilon$. This enables the transmission technique to be used for strain measurement or materials characterization. However, such measurements have already been achieved by traditional neutron diffraction, so why use the transmission method? The transmission method has two unique features that provide advantages in specific cases. Firstly, TOF neutron transmission can produce two-dimensional images depicting the changes in the lattice parameter across the sample area in a way similar to neutron radiography. This has an important application in neutron stress scanning because it can provide a fast determination of the unstressed lattice parameter in cases where there is a likelihood of compositional variations, such as in welds or heat-treated zones. To facilitate such measurement, a new detector bank comprising an array of 10 × 10 4 mm^2 scintillating detectors is currently under development; its predicted performance for the determination of the lattice parameters of different materials is given in Table 1. The second big advantage of the transmission technique lies in the very fast rate of data acquisition, which has been exploited previously by Meggers *et al.* (1994) and by Vogel (2000) to study the kinetics of the austenite–bainite phase transformation in steel. In these works, the height of the Bragg edges associated with each phase or a complete Rietveld refinement of the spectra were used to provide quantitative phase analysis (QPA) as a function of time.

Furthermore, the nuclear absorption resonances appearing in the short-wavelength range of the transmitted neutron spectra can be used to gather information about impurities present in the sample or, after attaching a very thin foil of tantalum or rhenium, the temperature of the sample (Mayers *et al.*, 1989). So, if high spatial resolution is not required, bulk samples can be characterized by TOF neutron transmission in very short times. As a rough calculation, the total area of 400 mm^2 obtained by adding together the counts of the 100 elements of the new detector bank, gives a predicted data

Table 1
Predicted performance of the transmission diffractometer for the first Bragg edge of different materials and experimental conditions.

Better results would be achieved by Pawley-type multiple-edge refinements.

				Resolution $\Delta d/d$ ($\times 10^{-4}$) with optimal thickness		Counting time required for $\Delta d/d = 10^{-4}$ with a 400 mm^2 detector (s)	
Element	σ_0 (barns)	σ_{hkl} (barns)	Optimal thickness (cm)	1 h, 4 mm^2	10 s, 400 mm^2	Optimal thickness	5 mm
Fe (b.c.c.)	6.59	14.47	1.58	0.7	1.3	18	47
Fe (f.c.c.)	6.86	10.44	2.25	0.9	1.7	28	121
Copper	9.76	6.85	1.72	1.4	2.7	72	209
Nickel	15.92	12.49	0.95	1.3	2.4	60	85
Aluminium	0.72	3.95	11.85	0.6	1.2	14	1050
Lead	1.27	10.0	9.35	0.7	1.5	21	970
Zirconium	3.26	5.59	7.20	1.0	1.9	13	440
Niobium	3.27	8.04	4.58	0.8	1.5	24	338

acquisition rate of 1600 neutrons s^{-1} for a time channel of 0.001 resolution at 2 Å. This enables the measurement of the transmission spectrum of a 1.6 cm thick sample of austenitic steel in 5 s with 1% uncertainty.

Despite this very fast rate of data acquisition, the small gauge volumes and thin samples required for unstressed lattice-parameter determination in engineering applications results in a relatively poor signal to noise ratio and much longer measurement times are required for reliable application of the technique. The same circumstances appear in quantitative phase analysis when one of the phases is present in low concentration; hence an analysis combining the information from all the edges could significantly improve the statistical accuracy of the resulting lattice parameter or phase fraction. Moreover, by including as many reflections as possible in the data analysis, the results are less likely to be affected by preferred orientation effects, providing values more representative of the macroscopic (engineering) properties of the sample.

The most efficient approach to follow in each case is, however, different. In the stress determination of engineering components, only changes in lattice parameters are required from the experiment. Hence, the method proposed by Pawley (1981), linking the positions of the edges to a single set of lattice parameters but leaving the heights of the edges unconstrained, can be adopted for this purpose (Steuwer *et al.*, 2000). As noted in Fig. 6(*a*), multiple-edge refinements should be limited to those edges having $2d_{hkl} > 1.3$ Å, and the position of the edges in the TOF scale should be defined using equation (15). A more accurate model for the TOF wavelength scale must be adopted if more reflections are to be included in the analysis. As the information about lattice parameter is contained only in the Bragg edges, the least-squares refinement can be restricted to the signal in the immediate neighbourhood of the edges and the fitting performed following the three stages described in §3. So, after completing the first two stages for each individual edge, the position of all edges should be refined simultaneously by fitting a unique set of lattice parameters while the decay constant τ is fixed to the value defined during the calibration of the instrument. This Pawley-type approach has been successfully applied to the determination of the unstressed lattice parameter (Steuwer *et al.*, 2000).

By contrast, the intensity of the edges is the relevant magnitude in quantitative phase analysis. Accordingly, the intensity of each reflection must be calculated from the motif of the atoms in the unit cell and from the orientation distribution function (ODF) of the crystallites composing the sample. This is the approach adopted in Rietveld refinement of diffraction data, but the equivalence is not complete because the effect of the non-coherent and inelastic scattering on the transmission of the sample is neither small, nor a simple function of the neutron wavelength. So, if the phase fraction is the only required information, or the other contributions to the total cross section are not exactly known, the least-squares fitting should also be limited to the immediate vicinity of the edges. In terms of the ideas presented in §3, in QPA the values of σ_{hkl} appearing in equation (7) must be calculated from the positions of the atoms in the unit cell and from the ODF of the sample, which have then to be refined together with the lattice parameters.

8. Conclusion

It has been shown that the position of the Bragg edges appearing in TOF neutron spectra transmitted by polycrystalline materials can be used to define interplanar distances to an uncertainty of 0.0001 Å. A comprehensive description of the broadening of the Bragg edges as a result of the instrumental uncertainties intrinsic to the TOF technique has been presented, leading to the development of a simple model to describe analytically the edge line shape. The capability of this model to provide reliable values of the interplanar distances has been proved by a comparison of transmission and diffraction experiments on reference samples and from a study of the possible systematic errors. The effect of sample thickness on the sensitivity of a transmission diffractometer has been studied and an optimal thickness depending on the density and the cross sections of a material has been defined. The capability of the present instrument for strain analysis has been demonstrated and, finally, the performance and the possible range of applications of a future transmission diffractometer provided with a pixellated detector have been discussed.

The authors wish to thank M. E. Fitzpatrick, M. W. Johnson, F. Kropff, J. R. Granada, H. G. Priesmeyer and S. Vogel for helpful discussion of this work, M. R. Daymond for his invaluable assistance during the experiments, N. Rhodes for the design of the transmission detector, D. Q. Wang for the measurement of the Poisson ratio data, and P. Ledgard for the preparation of the samples and the stress rig. This work has been supported by EPSRC, the UK Engineering and Physical Sciences Research Council.

References

Carpenter, J. M., Mueller, M. H., Beyerlein, R. A., Worlton, T. G., Jorgensen, J. D., Brun, T. O., Sköld, K., Pelizzari, C. A., Peterson, S. W., Watanabe, N., Kimura, M. & Gunning, J. E. (1975). *Proceedings of Neutron Diffraction Conference, Petten, The Netherlands,* pp. 192–208. Reactor Centrum Nederland, RCN-234.

CRC Handbook of Chemistry and Physics (1997). 78th ed., edited by D. R. Lide, pp. 12–21. Boca Raton, New York: CRC Press.

Granada, J. R., Santisteban, J. R. & Mayer, R. E. (1995). *Physica B*, **213&214**, 1005–1007.

Hiismäki, P. (1988). *J. Appl. Cryst.* **22**, 79–83.

Johnson, M. W., Edwards, L. & Withers, P. J. (1997). *Physica B*, **234**, 1141–1143.

Kropff, F. & Granada, J. R. (1975). *CRIPO. Program for total cross section calculation of polycrystalline materials*. Centro Atómico Bariloche, CNEA, Argentina.

Kropff, F., Granada, J. R. & Mayer, R. E. (1982). *Nucl. Instrum. Methods*, **198**, 515–521.

Mayers, J., Baciocco, G. & Hannon, A. C. (1989). *Nucl. Instrum. Methods A*, **275**, 453–459.
Meggers, K., Priesmeyer, H. G., Trela, W. G. & Dahms, M. (1994). *Mater. Sci. Eng. A*, **188**, 301–304.
Pawley, G. S. (1981). *J. Appl. Cryst.* **14**, 357–361.
Smithells Metals Reference Book (1983). 6th ed., edited by E. A. Brandes. London: Butterworths.
Steuwer, A., Withers, P. J., Santisteban, J. R., Edwards, L., Fitzpatrick, M. E., Daymond, M. R., Johnson, M. W. & Bruno, G. (2000). *Proceedings of the Sixth International Conference of Residual Stresses*. Oxford: IOM Communications.
Strunz, P., Lukáš, P., Mikula, P., Wagner, V., Kouril, Z. & Vrána, M. (1997). *Proceedings of the Fifth International Conference of Residual Stresses, Linköping, Sweden*. Linköping University Press.
Vogel, S. (2000). PhD thesis, Christian-Albrechts-Universitat, Kiel, Germany.
Wang, D. Q. (1996). PhD thesis, The Open University, UK.
Windsor, C. G. & Izuyama, T. (1992). *Measurement of Residual and Applied Stress Using Neutron Diffraction*, edited by M. T. Hutchings & A. D. Krawitz, pp. 147–158. Dordrecht: Kluwer Academic Publishers.